# Supporting Information

# Interactions between nanoscale zerovalent iron (NZVI) and silver nanoparticles alter the NZVI reactivity in aqueous environments

Junmin Deng[1], Sunho Yoon[2], Mathieu Pasturel[3], Sungjun Bae[2*], Khalil Hanna[1*]

[1] *University of Rennes, Ecole Nationale Supérieure de Chimie de Rennes, CNRS, ISCR-UMR 6226, F-35000, Rennes, France*

[2] *Department of Civil and Environmental Engineering, Konkuk University, 120 Neungdong-ro, Gwangjin-gu, Seoul 05029, Republic of Korea*

[3] *Univ. Rennes, CNRS, ISCR – UMR 6226, F-35000, Rennes, France*

*Co-corresponding authors: khalil.hanna@ensc-rennes.fr and bsj1003@konkuk.ac.kr

17 pages; 3 Tables; and 11 Figures.

# Supporting Information

## Table of contents

# Supporting Information

**Table S1**. *p*-NP and *p*-AP concentrations after the reaction in different reaction systems

| Reaction systems | *p*-NP concentration after reaction(mM) | *p*-AP concentration after reaction (mM) |
|---|---|---|
| NZVI (25 mg·$L^{-1}$) | 0.02824 | 0.06982 |
| NZVI (50 mg·$L^{-1}$) | 0 | 0.1009 |
| AgNPs (10 mg/L) | 0.10003 | 0 |
| NZVI (25 mg·$L^{-1}$) + AgNPs (0.5 mg·$L^{-1}$) | 0.03757 | 0.06403 |
| NZVI (25 mg·$L^{-1}$) + AgNPs (2 mg·$L^{-1}$) | 0.03608 | 0.06382 |
| NZVI (25mg·$L^{1}$) + AgNPs (10 mg·$L^{-1}$) | 0.01624 | 0.08607 |
| NZVI (25 mg·$L^{-1}$) + AgNPs (25 mg·$L^{-1}$) | 0.01125 | 0.08958 |
| NZVI (25 mg·$L^{-1}$) + AgNPs (50 mg·$L^{-1}$) | 0.00688 | 0.09142 |
| NZVI (50 mg·$L^{-1}$) + AgNPs (0.5 mg·$L^{-1}$) | 0.04709 | 0.05504 |
| NZVI (50 mg·$L^{-1}$) + AgNPs (2 mg·$L^{-1}$) | 0.03277 | 0.06995 |
| NZVI (50 mg·$L^{-1}$) + AgNPs (10 mg·$L^{-1}$) | 0.01475 | 0.08373 |
| NZVI (50 mg·$L^{-1}$) + AgNPs (25 mg·$L^{-1}$) | 0.01204 | 0.08722 |
| NZVI (50 mg·$L^{-1}$) + AgNPs (50 mg·$L^{-1}$) | 0 | 0.09837 |
| NZVI (50 mg·$L^{-1}$) + AgNPs (100 mg·$L^{-1}$) | 0 | 0.1002 |
| NZVI (25 mg·$L^{-1}$) + $TiO_2$ (5 mg·$L^{-1}$) | 0.04202 | 0.05921 |
| NZVI (25 mg·$L^{-1}$) + $TiO_2$ (10 mg·$L^{-1}$) | 0.039 | 0.06176 |
| NZVI (25mg·$L^{1}$) + $TiO_2$ (25 mg·$L^{-1}$) | 0.02894 | 0.073 |
| NZVI (25 mg·$L^{-1}$) + $TiO_2$ (50 mg·$L^{-1}$) | 0.02769 | 0.07289 |
| NZVI (25 mg·$L^{-1}$) + $TiO_2$ (100 mg·$L^{-1}$) | 0.01914 | 0.08001 |
| NZVI (50 mg·$L^{-1}$) + $TiO_2$ (5 mg·$L^{-1}$) | 0.02325 | 0.07524 |
| NZVI (50 mg·$L^{-1}$) + $TiO_2$ (10 mg·$L^{-1}$) | 0.00069 | 0.09792 |
| NZVI (50 mg·$L^{-1}$) + $TiO_2$ (25 mg·$L^{-1}$) | 0 | 0.10086 |
| NZVI (50 mg·$L^{-1}$) + $TiO_2$ (50 mg·$L^{-1}$) | 0 | 0.09806 |
| NZVI (50 mg·$L^{-1}$) + $TiO_2$ (100 mg·$L^{-1}$) | 0 | 0.09939 |
| NZVI (50 mg·$L^{-1}$) + FB sand (2 mg·$L^{-1}$) | 0 | 0.101 |

| | | |
|---|---|---|
| NZVI (50 mg·$L^{-1}$) + FB sand (10 mg·$L^{-1}$) | 0 | 0.1003 |
| NZVI (50 mg·$L^{-1}$) + FB sand (25 mg·$L^{-1}$) | 0 | 0.0996 |
| NZVI (50 mg·$L^{-1}$) + FB sand (50 mg·$L^{-1}$) | 0 | 0.09719 |
| NZVI (50 mg·$L^{-1}$) + FB sand (100 mg·$L^{-1}$) | 0 | 0.09833 |
| NZVI (50 mg·$L^{-1}$) + $Na^{+}$/$Cl^{-}$ | 0 | 0.09785 |
| NZVI (50 mg·$L^{-1}$) + $SO_4^{2-}$ | 0.0008 | 0.0979 |
| NZVI (50 mg·$L^{-1}$) + $NO_3^{-}$ | 0.05622 | 0.04182 |
| NZVI (50 mg·$L^{-1}$) + $SiO_3^{2-}$ | 0.01564 | 0.08505 |
| NZVI (50 mg·$L^{-1}$) + $Ca^{2+}$ | 0 | 0.0985 |
| NZVI (50 mg·$L^{-1}$) + $Mg^{2+-}$ | 0 | 0.1018 |
| NZVI (50 mg·$L^{-1}$) + HA | 0 | 0.09932 |
| NZVI (50 mg·$L^{-1}$) + AgNPs (10 mg·$L^{-1}$) + $Na^{+}$/$Cl^{-}$ | 0.01554 | 0.08754 |
| NZVI (50 mg·$L^{-1}$) + AgNPs (10 mg·$L^{-1}$) + $SO_4^{2-}$ | 0 | 0.0979 |
| NZVI (50 mg·$L^{-1}$) + AgNPs (10 mg·$L^{-1}$) + $NO_3^{-}$ | 0.07911 | 0.0218 |
| NZVI (50 mg·$L^{-1}$) + AgNPs (10 mg·$L^{-1}$) + $SiO_3^{2-}$ | 0.03323 | 0.06505 |
| NZVI (50 mg·$L^{-1}$) + AgNPs (10 mg·$L^{-1}$) + $Ca^{2+}$ | 0.02697 | 0.07395 |
| NZVI (50 mg·$L^{-1}$) + AgNPs (10 mg·$L^{-1}$) + $Mg^{2+}$ | 0.01699 | 0.08532 |
| NZVI (50 mg·$L^{-1}$) + AgNPs (10 mg·$L^{-1}$) + HA | 0 | 0.1002 |

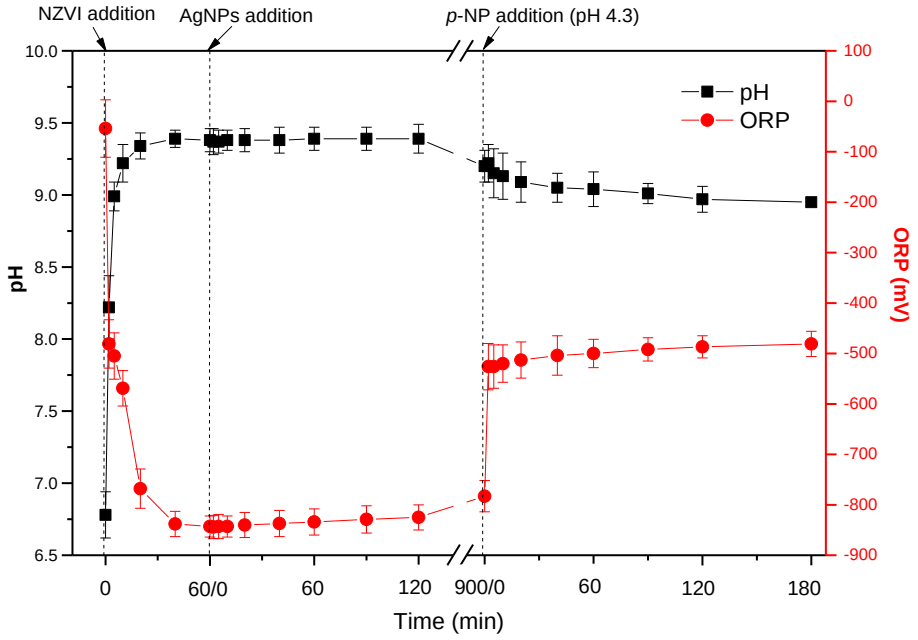


**Fig. S1**. Variations in solution pH and ORP during the experiment in NZVI+AgNPs system. Experimental conditions: $[p\text{-NP}]_{initial}$ = 0.1 mM, [NZVI]= 50 mg/L, [AgNPs]= 10 mg/L. No ferrous ion has been detected in solution under these conditions

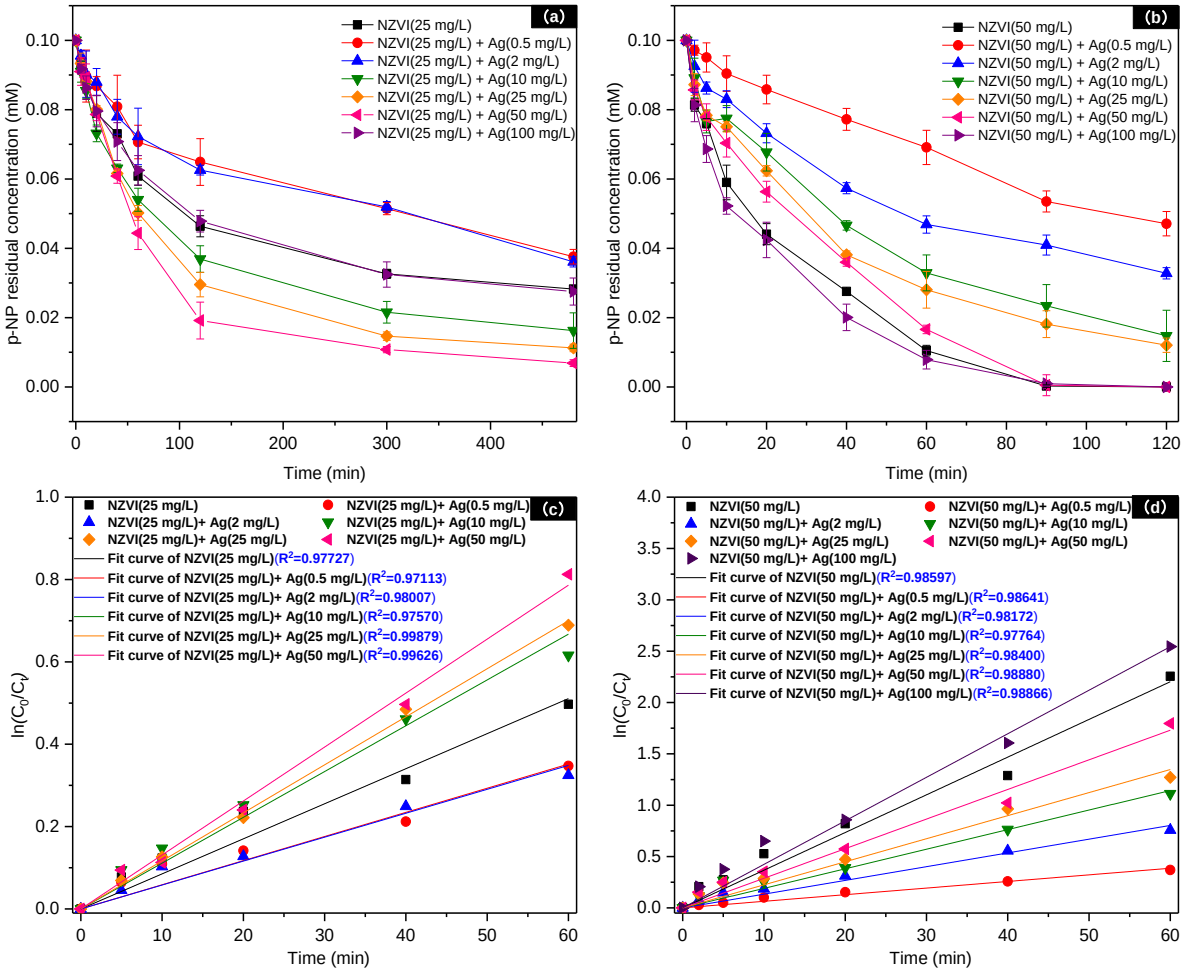


**Fig. S2.** The removal kinetics of *p*-NP by NZVI with different dose of AgNPs at (a) 25 mg/L NZVI and (b) 50 mg/L NZVI; (c) and (d) the corresponding kinetic modeling for the first 60 mins in the reaction. Experimental conditions: $[p\text{-NP}]_{initial}$ = 0.1 mM, reaction pH=9.0±0.2.

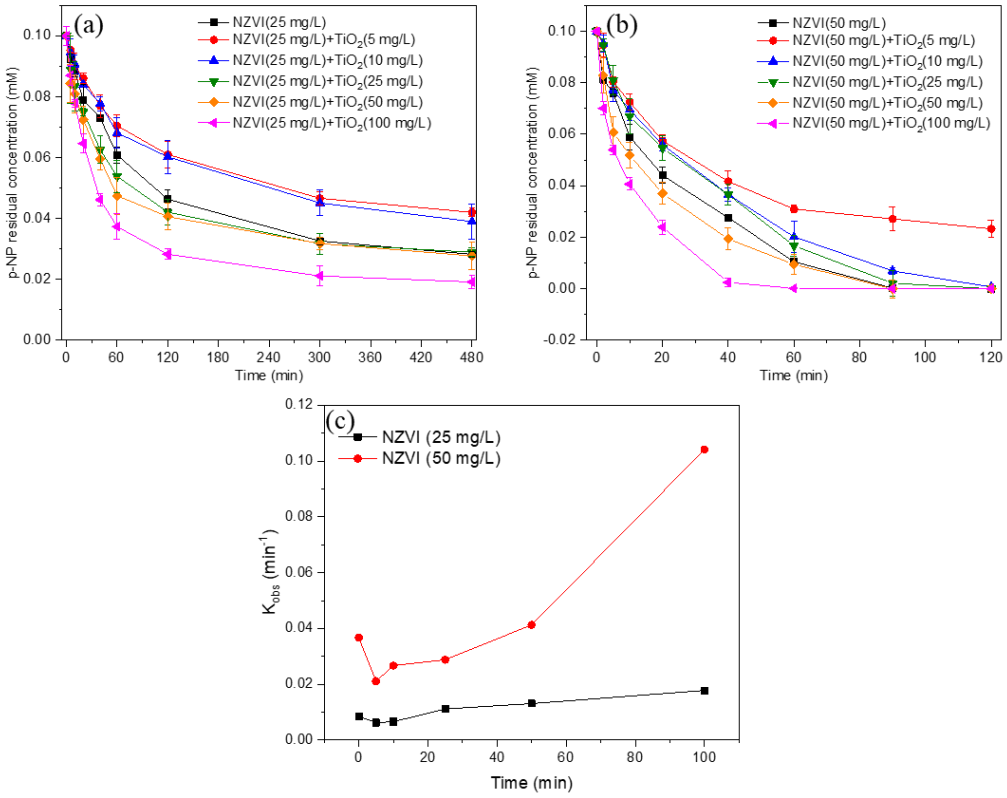


**Fig. S3.** The removal kinetics of *p*-NP by NZVI with different dose of $TiO_2$ nano particles at (a) 25 mg/L NZVI and (b) 50 mg/L NZVI; and (c) the variation of pseudo-first-order kinetic rate constants ($k_{obs}$, $min^{-1}$) with respect to dosage of $TiO_2$ nanoparticles. Experimental conditions: $[p\text{-NP}]_{initial}$ = 0.1 mM, reaction pH=9.0±0.2.

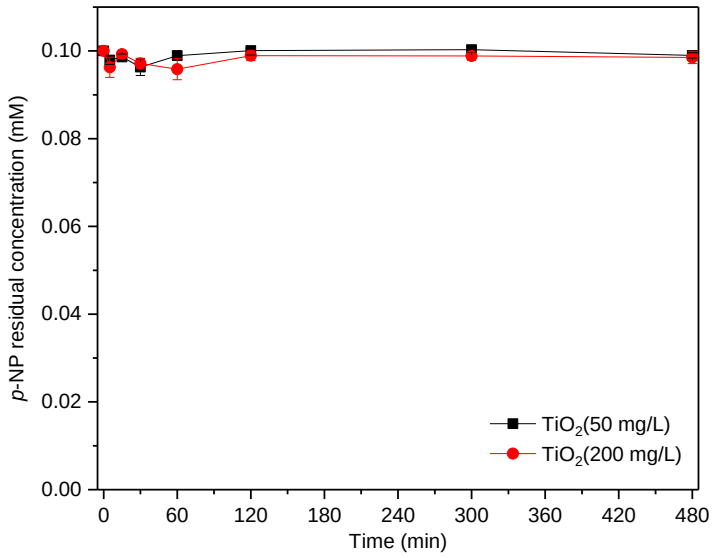


**Fig. S4.** The removal kinetics of *p*-NP by different dose of $TiO_2$ nano particles. Experimental conditions: $[p\text{-NP}]_{initial}$ = 0.1 mM, reaction pH=9.0±0.2.

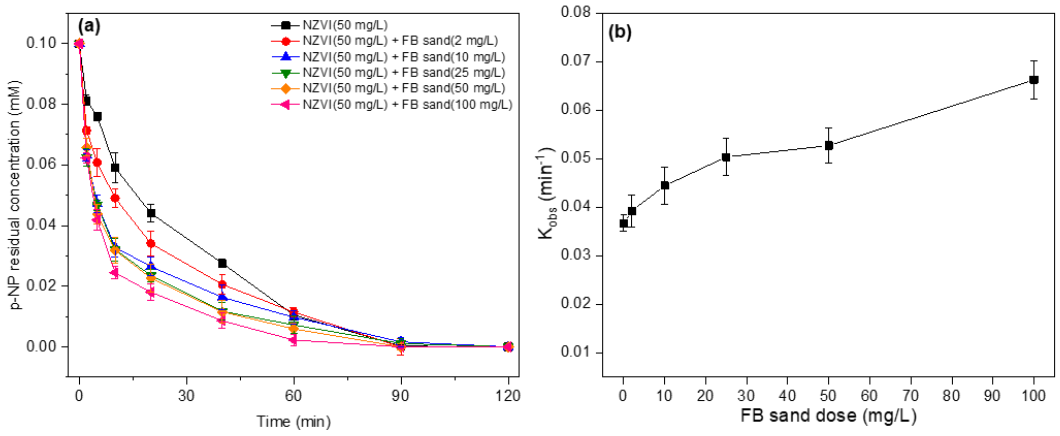


**Fig. S5.** (a) The removal kinetics of *p*-NP by NZVI with different dose of FB sand, and (b) the variation of pseudo-first-order kinetic rate constants ($k_{obs}$, $min^{-1}$) with respect to FB sand dosage. Experimental conditions: $[p\text{-NP}]_{initial}$ = 0.1 mM, reaction pH=9.0±0.2.

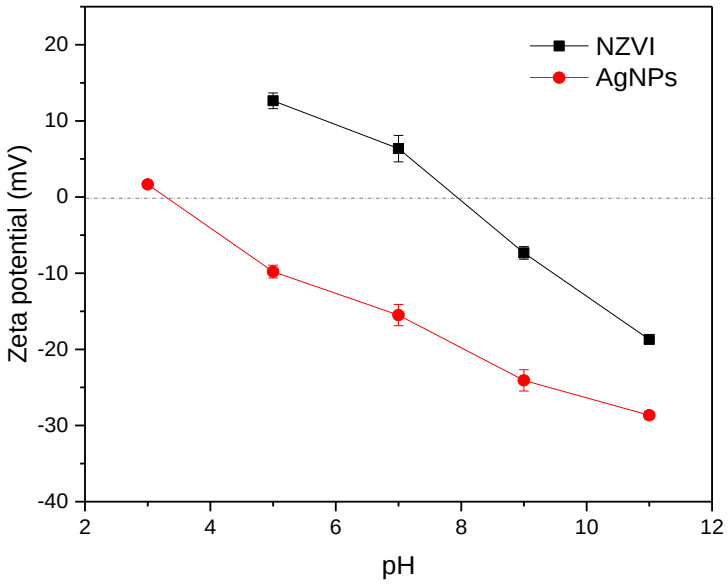


**Fig. S6.** The zeta potential of NZVI and AgNPs at different pHs.

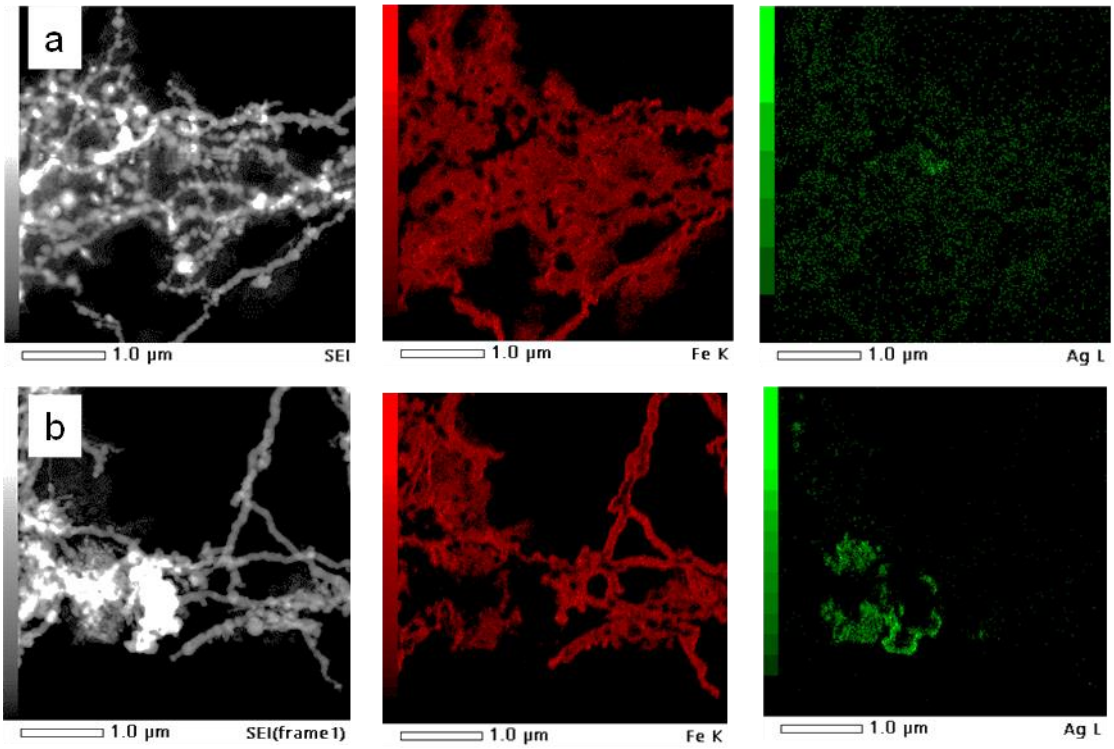


**Fig. S7.** TEM images of (a) AgNP–NZVI at 10 mg/L AgNPs, and (b) AgNP–NZVI at 100 mg/L AgNPs after the *p*-NP reduction. Conditions: [NZVI] = 50 mg/L.

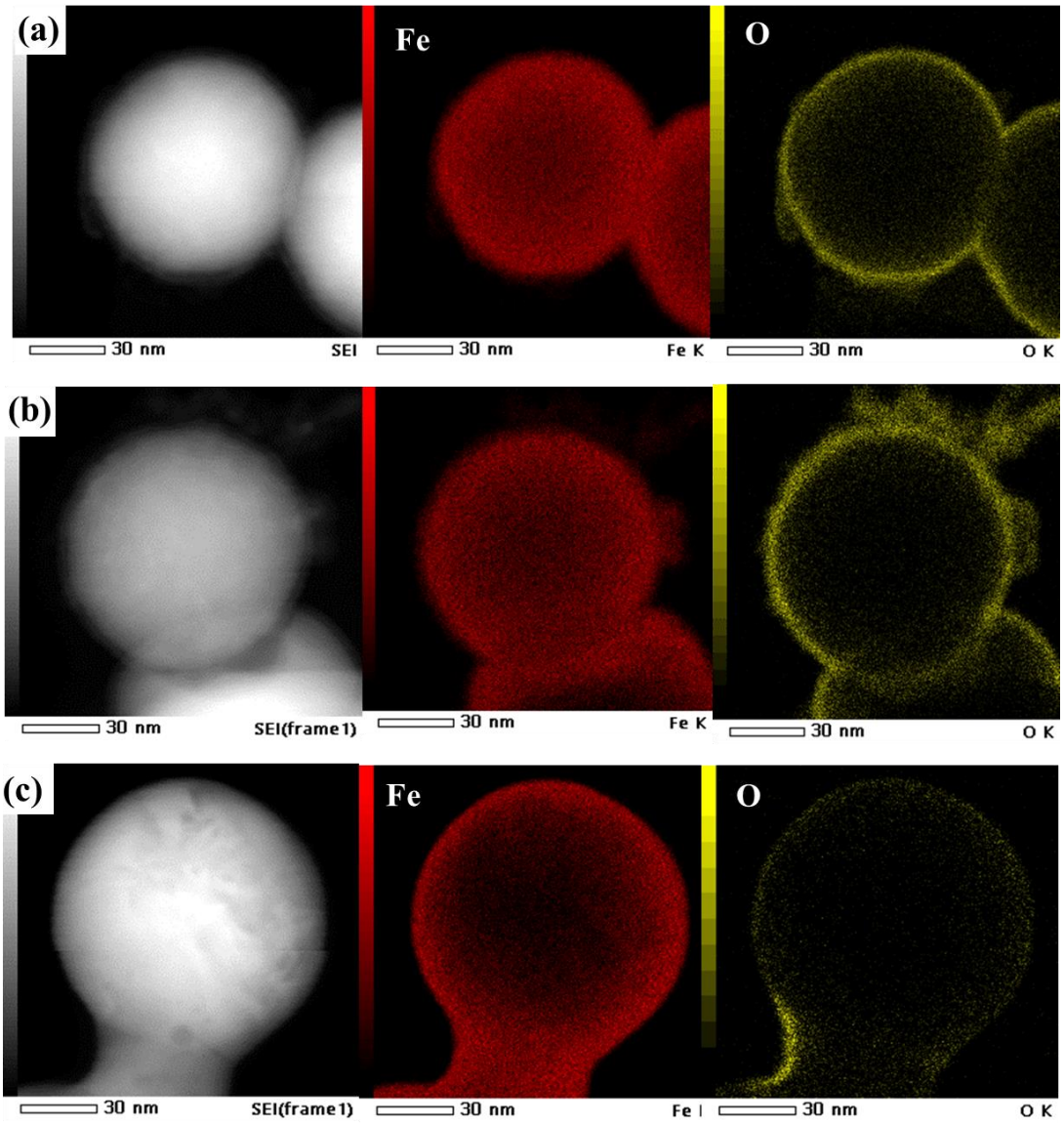


**Fig. S8.** TEM images and the elemental mapping of NZVI particles in different reaction systems (a) bare NZVI, (b) AgNPs–NZVI at 10 mg/L AgNPs and (c) AgNPs–NZVI at 100 mg/L AgNPs. Conditions: [NZVI]=50 mg/L.

# Supporting Information

**DLVO theory:** The DLVO (Derjaguin, Landau, Verwey and Overbeek) theory was employed to estimate the stability of the NZVI and AgNPs in the suspensions. This theory takes into account attractive van der Waals (vdW) and repulsive electrostatic double-layer (EDL) forces between the particles ($\Phi_{DLVO} = \Phi_{EDL} + \Phi_{vdW}$). Since the particles of AgNPs and NZVI were both spherical, the vdW and EDL interaction energies for the AgNP-AgNP, NZVI-AgNPs, and NZVI-NZVI systems were calculated according to the sphere-sphere equation. The expressions for calculating the vdW interaction energy ($\Phi_{vdW}$) for the sphere-sphere are presented in Eq. (S1) (Elimelech et al., 1995; Tong et al., 2008).

$$\Phi_{vdW} = -\frac{A_{132}\, r_{h1} r_{h2}}{6h(r_{h1}+r_{h2})}\left(1+\frac{14h}{\lambda}\right)^{-1} \quad \text{(S1)}$$

where $r_{h1}$ and $r_{h2}$ in Eq. (S1) refer to the average hydrodynamic radii of the two interacting particles (AgNPs and NZVI) (see Table S1); h is the separation distance between two particles; λ is the characteristic wavelength of the interaction (usually 100 nm); $A_{132}$ is the Hamaker constants for AgNPs-water-AgNPs, NZVI-water-NZVI or AgNPs-water-NZVI, which is obtained from the Hamaker constants of the individual phase using Eq. (S2) (Wang et al., 2019).

$$A_{132} = (\sqrt{A_1} - \sqrt{A_{water}})(\sqrt{A_2} - \sqrt{A_{water}}) \quad \text{(S2)}$$

where $A_1$ and $A_2$ is the Hamaker constant of the two particles ($A_{AgNPs} = 6.99\times10^{-20}$ J[3] and $A_{NZVI} = 10^{-19}$ J[4]) (Kocur et al., 2013). The EDL interaction energy ($\Phi_{EDL}$) for the sphere-sphere configurations can be calculated using Eq.(S3) (Wang et al., 2019).

$$\Phi_{EDL} = 0.5\pi\varepsilon_0\varepsilon_r \frac{r_{h1} r_{h2}}{(r_{h1}+r_{h2})}\left\{2\psi_1\psi_2 ln\left[\frac{1+\exp(-kh)}{1-\exp(-kh)}\right] + (\psi_1{}^2 + \psi_2{}^2) ln[1 - \exp(-2kh)]\right\} \quad \text{(S3)}$$

where $\varepsilon_0$ and $\varepsilon_r$ are the dielectric permittivity of the vacuum (8.854×10−12 C/Vm) and water (78.5 at 298 K), respectively; ψ1 and ψ2 are the zeta-potentials of the two interact particles, κ is the Debye-Hückel parameter, which is calculated using Eq. (S4) (Wang et al., 2019).

$$k = \sqrt{\frac{1000e^2 \sum n_{j0} z_j{}^2}{\varepsilon_0\varepsilon_r KT}} \quad \text{(S4)}$$

where, e is the electron charge ($1.602\times10^{-19}$ C); $n_{j0}$ is the number concentration of the ion in the bulk suspension ($6.022\times10^{23}$ $mol^{-1}$); $z_j$ is the ion valence; K is the Boltzmann constant ($1.38\times10^{-23}$ J/K); and T is the absolute temperature (298 K).

Based on the determined average hydrodynamic diameter ($D_h$) and zeta -potentials of AgNPs and NZVI (Table S2), the interaction energies of AgNPs-AgNPs and NZVI-AgNPs at different AgNPs loadings were calculated (Fig. S6). The calculated maximum repulsive energy barrier and attractive secondary minimum are listed in Table S3. The calculation indicated the shallow attractive secondary minimums ($\Phi_{min2}$, less than 0.2 kT units) in all cases, which is too low for the flocculation (Tadros, 2014). Thus, the weak and reversible flocculation caused by secondary minimums will not be taken into

our consideration. The calculated maximum repulsive interaction energies ($\Phi_{max}$) values were all positive, suggesting that the particles are not expected to be aggregated (i.e., overcome the repulsive energy barrier). However, the aggregate forms can be easily found in many literatures and even in our TEM images. This might be induced by that classical DLVO does not consider non-DLVO factors such as solution chemistry and magnetic property (Grasso et al., 2002), which cannot be completely eliminated in our experimental systems. Therefore, it might be possible that these particles could overcome the repulsive energy barrier and assembly to form lager structures when the repulsive energy barrier is low.

At low AgNPs loading (10 mg/L), repulsive energy barriers were 12.36 kT for AgNPs–AgNPs, 3.51 kT for AgNPs–NZVI, and 1.09 kT for NZVI–NZVI. The $\Phi_{max}$ values of AgNPs–NZVI and AgNPs–AgNPs were relatively low that could be easily overcome and reached the primary energy well, indicating the possible occurrences of heteroaggregation (AgNPs–NZVI) and homoaggregation (NZVI- NZVI). On the other hand, the high repulsive energy barriers of AgNPs–AgNPs make it difficult for AgNPs homoaggregation. With increasing AgNPs dose (100 mg/L), for either homoaggregation (AgNPs–AgNPs) or heteroaggregation (AgNPs–NZVI), the magnitude of $\Phi_{max}$ increased substantially. The repulsive energy barriers for AgNPs–AgNPs and AgNPs–NZVI were 80.06 kT and 11.82 kT, respectively. It would not be sufficient non-DLVO energy to overcome the repulsive energy barrier for heteroaggregation (AgNPs–NZVI), suggesting lower degree of heteroaggregation and homoaggregation (AgNPs–AgNPs) at high AgNPs loading over lower AgNPs loading.

**Table S2**. Average hydrodynamic diameter (Dh) and zeta -potentials of the AgNPs and NZVI used in DLVO calculations in different experimental conditions. Conditions: pH 9.

| Experimental conditions | Dh(nm) | zeta potentials(mV) |
|---|---|---|
| **AgNPs(10 mg/L)** | 200.1 | -20.1 |
| **AgNPs(100 mg/L)** | 778.7 | -20.1 |
| **NZVI (50 mg/L)** | 593.4 | -7.33 |

**Table S3.** Calculated DLVO interaction energies based on the different experimental conditions.

| | $\Phi_{max}$[a](KT) | $\Phi_{min2}$[b](KT) |
|---|---|---|
| **AgNPs(10mg/L)-AgNPs(10mg/L)** | 12.36048 | -0.00351 |
| **AgNPs(10mg/L)-NZVI(50mg/L)** | 3.50915 | -0.01524 |
| **NZVI(50mg/L)- NZVI(50mg/L)** | 1.088387 | -0.14654 |
| **AgNPs(100mg/L)-AgNPs(100mg/L)** | 80.05521 | -0.02274 |
| **AgNPs(100mg/L)-NZVI(50mg/L)** | 11.82193 | -0.05133 |

a $\Phi_{max}$ is maximum repulsive energy barrier; b $\Phi_{min2}$ is attractive secondary minimum; K is the Boltzmann constant (1.38×10.23 J/K), and T is the absolute temperature (298 K).

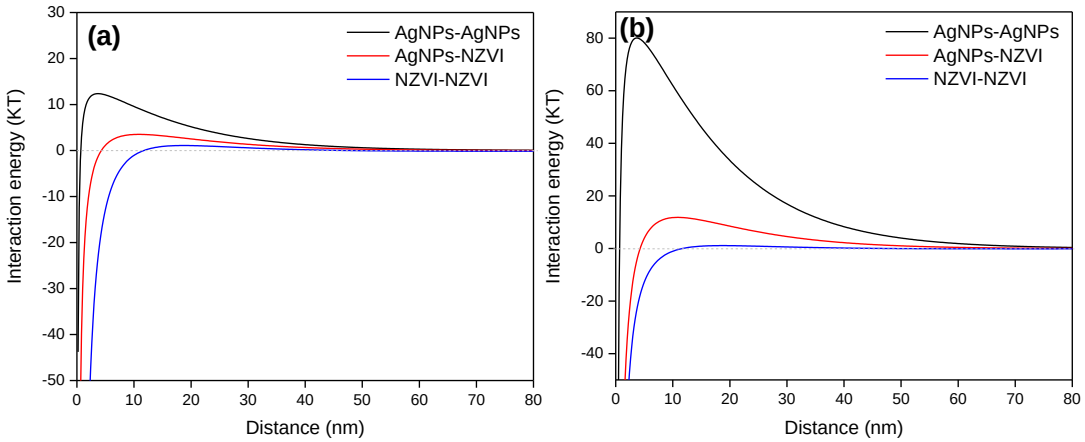


**Fig. S9.** Calculated DLVO interaction energy profiles of AgNPs-AgNPs, AgNPs-NZVI and NZVI-NZVI at the AgNPs concentration of (a) 10 mg/L and (b) 100 mg/L Conditions: [NZVI]=50 mg/L, pH 9.

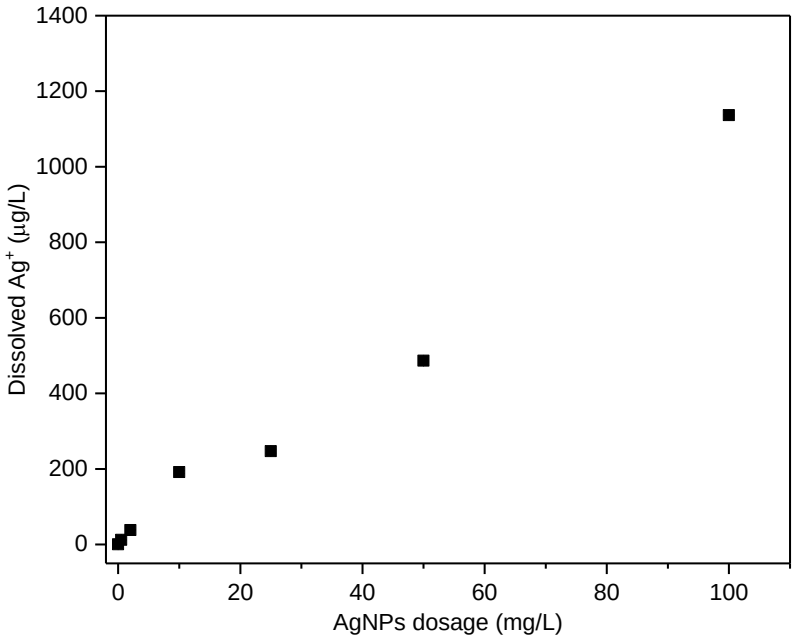


**Fig. S10.** $Ag^{+}$ release of AgNPs suspensions after 3 days at different AgNPs dosage at pH 9.

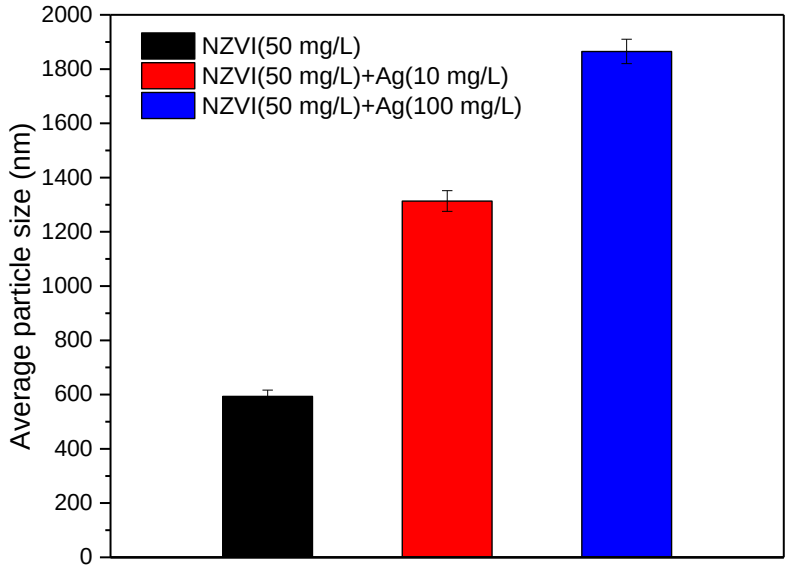


**Fig. S11**. Average particle size of NZVI and AgNPs–NZVI complexes.

**References**

Elimelech, M., Gregory, J., Jia, X., Williams, R.A., 1995. CHAPTER 6 - Modelling of aggregation processes, in: Elimelech, M., Gregory, J., Jia, X., Williams, R.A. (Eds.), Particle Deposition and Aggregation. Butterworth-Heinemann, pp. 157-202.

Grasso, D., Subramaniam, K., Butkus, M., Strevett, K., Bergendahl, J., 2002. A review of non-DLVO interactions in environmental colloidal systems. Reviews in Environmental Science and Biotechnology 1(1), 17-38.

Kocur, C.M., O'Carroll, D.M., Sleep, B.E., 2013. Impact of nZVI stability on mobility in porous media. J. Contam. Hydrol. 145, 17-25.

Tadros, T., 2014. Colloid and interface aspects of pharmaceutical science, Colloid and Interface Science in Pharmaceutical Research and Development. Elsevier, pp. 29-54.

Tong, M., Ma, H., Johnson, W.P., 2008. Funneling of Flow into Grain-to-grain Contacts Drives Colloid−Colloid Aggregation in the Presence of an Energy Barrier. Environ. Sci. Technol. 42(8), 2826-2832.

Wang, R., Dang, F., Liu, C., Wang, D.-j., Cui, P.-x., Yan, H.-j., Zhou, D.-m., 2019. Heteroaggregation and dissolution of silver nanoparticles by iron oxide colloids under environmentally relevant conditions. Environmental Science: Nano 6(1), 195-206.

Xu, Y., Tang, H., Liu, J.-h., Wang, H., Liu, Y., 2013. Evaluation of the adjuvant effect of silver nanoparticles both in vitro and in vivo. Toxicol. Lett. 219(1), 42-48.